ELSEVIER

Chemical Engineering Journal 70 (1998) 55–64

Chemical Engineering Journal

Modelling of crystalline layer growth using kinetic data obtained from suspension crystallization

S. Briançon *, D. Colson, J.P. Klein

Laboratoire d'Automatique et de Génie des Procédés (LAGEP), UPRES-A CNRS Q5007 Université Claude Bernard Lyon 1, CPE Lyon, Villeurbanne, France

Received 14 April 1997; revised 26 September 1997; accepted 5 January 1998

Abstract

The fouling of cooling surfaces of industrial crystallizers is a major problem which reduces the productivity of installations. This phenomenon is initiated by primary heterogeneous nucleation at the wall, followed by growth, leading to the formation of a crystalline layer which increases the thermal resistance of the system. An experimental device was designed to study the conditions of appearance and subsequent growth of the layer. The influence of the main parameters was studied. Thermal modelling of fouling in an annular exchanger was performed, using the experimental results. This led to an evolution of the thickness of the layer with time and position. It also enabled the supersaturation profile to be calculated at any time, thus making the link between the growth of the layer and the kinetics of crystallization in suspension. Although a simplifying hypothesis was used for modelling, good agreement was obtained concerning the initial mass flow of crystallization, using growth rates obtained in suspension crystallization to calculate the growth in thickness of the layer.

Keywords: Fouling; Cooling crystallization; Heat exchange surface; Nucleation; Growth; Crystalline layer; Kinetics

1. Introduction

The fouling of cooling surfaces of crystallizers is an industrial problem of great importance, which results in a loss of productivity and, therefore, heavy economic penalties. This problem is also well known in the field of heat exchangers [1] using water-containing salts which can crystallize at a warm wall. In the case of cooling crystallization, encrustation is the direct outcome of the operating conditions. Indeed, the process requires cold exchange surfaces which provide the lowest temperature in the crystallizer. As a result of local supersaturation, nucleation occurs preferentially at the wall. This leads to the growth of a crystalline layer at the wall, the thickness and structure of which are dependent on the operating conditions. However, this layer results in a decrease in heat exchange through the wall, and hence a reduction in crystal production in the suspension.

The conditions for the formation of a crystalline layer at the wall, and its subsequent growth, depend on a large number of parameters [2], some of which are not independent. Of these, hydrodynamics and temperature conditions are of great importance. The physicochemical interactions between the wall (material and microporosity) and the crystals (chemical nature) are also key parameters. The influence of the main parameters on fouling is known experimentally and can be represented by empirical laws [2–4].

Empirical studies allow some operating conditions to be determined which avoid or at least reduce encrustation [5] for a specific process. The optimal conditions are often the result of a compromise between the loss of productivity due to fouling and the cost of application of preventive solutions, which are expensive and not numerous [6]. The objective is to avoid the growth of crystals at the wall, without modifying the crystal properties in the suspension.

It is necessary to study in detail the mechanisms involved in fouling, in order to achieve a better understanding of the phenomenon and to represent it by more fundamental laws. The aim of this work is to propose a global model of encrustation, which uses a bank of experimental data and is based on the evolution of heat exchanges. This model should enable the growth of the crystalline layer to be predicted and the result to be linked with the kinetics of growth in suspension inferred from the literature.

* Corresponding author. LAGEP, UCB Lyon 1, CPE Lyon, Bat. 308 G, 43 Bd. du 11 Novembre 1918, 69 622 Villeurbanne, France. Tel.: +33-04-72-43-18-54; fax: +33-04-72-43-16-82; e-mail: stefanie@lagep.univ-lyon1.fr

1385-8947/98/$19.00
PII S1385-8947(98)00080-1

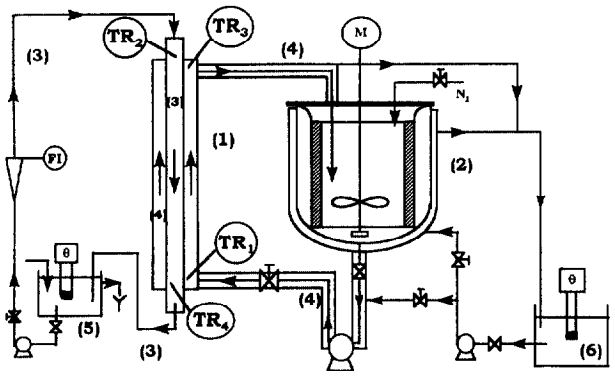

Fig. 1. Experimental set-up.

2. Experimental study

2.1. Experimental set-up

The experiments were performed in an annular crystallizer (1), shown in Fig. 1. The suspension flows in the annular space (4), whose inlet temperature and flow rate are kept constant. The cooling water counterflows in the inner tube (3), whose inlet temperature is controlled to the desired cooling rate, which is generally a linear slow decrease ($2°C\,h^{-1}$). This low value of the cooling rate was chosen such that, at any time, nearly steady state conditions prevail in the crystallizer. Crystallization occurs around the inner tube when the difference in temperature between the suspension and coolant reaches a critical value [7,8]. The experimental set-up and its operation are described in more detail elsewhere [7,8]. The chemicals studied in this work were adipic acid ($C_6H_{10}O_4$) and hydroquinone ($C_6H_6O_2$) in aqueous suspension.

2.2. Measurements

The inlet and outlet temperatures of the suspension (T_1 and T_3) and of the cooling water (T_2 and T_4) were continuously recorded. The evolution of these temperatures allows the variation of the overall heat exchange coefficient between the suspension and coolant to be measured continuously [7,8].

Experiments showed that the thickness of the layer was not homogeneous along the tube; therefore, we measured the evolution of the thickness versus z the position on the tube. The thickness and porosity profiles along the tube were measured at the end of each run by collecting the deposit and slicing it into small elements of about 0.05 m in length (the total length of the tube was 1 m).

The initiation of crystallization was characterized by the visual observation of the formation of the first crystals at the wall. The crystals always appeared first at the top of the crystallizer, corresponding to the outlet of the suspension. In this area, the temperature difference between the suspension and coolant is generally at its maximum value (about 0.2 K above the mean value). The higher supersaturation may therefore explain the initiation of crystallization at this point. To confirm this assumption, experiments were carried out in a parallel flow configuration, feeding the two flows at the bottom of the exchanger. In this case, the difference in temperature between the suspension and coolant is highest at the bottom of the crystallizer (inlet of the two flows). Nevertheless, the first crystals still appeared at the top of the crystallizer. These observations led to the conclusion that the dominant mechanisms are of hydrodynamic origin. Crystals do not appear first at the bottom of the crystallizer because turbulence is important at the inlet point, due to the lateral inlet of the suspension. Even when crystals are created or deposited on the tube, they will be rapidly removed by the suspension entering perpendicularly to the tube surface. In contrast, the first crystals appear at the top because, at this point, there is a turn around of the suspension before the outlet which increases the contact time between the suspension and the wall.

Following the formation of the first crystals at the top, a crystallization front appears, which then spreads along the tube under the influence of the increasing difference in temperature between the two fluids. Simultaneously, the crystals already formed keep growing, leading to the radial and axial development of the layer, the axial development increasing the front propagation rate. Visual observations of the displacement of this front lead in relationships of the form $t_0 = f(z)$, where t_0 is the time required for the first crystals to appear at position z. The position z is referenced with $z = 0$ at the bottom of the tube (entry of suspension) and $z = 1$ at the top.

2.3. Main operating conditions

Two kinds of experiments were performed.

2.3.1. Experiments with variable operating conditions

The results illustrate the influence of the operating factors on the main parameters which characterize fouling, such as the critical difference in temperature, mean thickness and porosity of the layer and displacement of the crystallization front [7].

The critical difference in temperature between the wall and the suspension is the value beyond which crystallization occurs at the wall. This critical difference in temperature is deduced from the observed thermal effect of fouling on the evolution of temperature in the crystallizer (see Section 3.3).

The mean thickness and porosity of the layer are the mean values obtained using the total weight of solids crystallized and considering a homogeneous thickness along the tube.

The displacement of the crystallization front ($t_0 = f(z)$ relationship) is measured for each run to obtain the influence of the operating conditions on the time of formation of the first crystals, on the one hand, and the rate of propagation of the front on the other.

The evolution of all of these parameters is measured in relation to the following variables: the temperature and mean

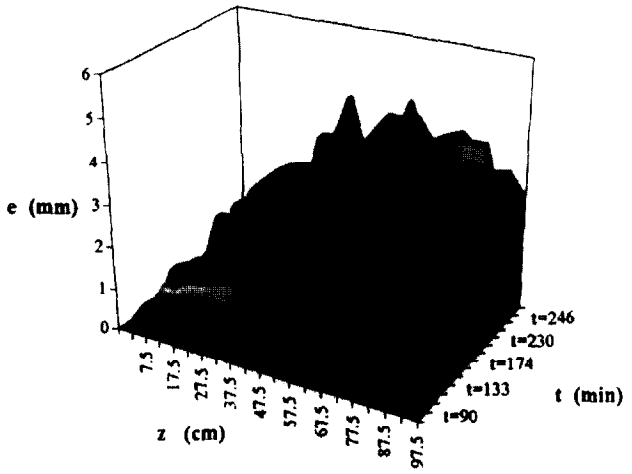

Fig. 2. Evolution of the thickness profiles with time.

velocity of the suspension, nature and surface finish of the inner tube and chemical nature of the crystals. The results are used to propose empirical laws to represent the influence of the operating parameters on the critical difference in temperature and the thickness and structure of the layer. These relations are then used for thermal modelling of the growth of the layer [7].

2.3.2. Experiments performed under constant conditions but with variable duration

This type of experiment leads to the evolution of thickness and porosity profiles with time under these specific conditions (see Fig. 2). In addition, the reproducibility of the initiation of fouling can be checked.

3. Modelling

3.1. Thermal balances

The thermal modelling of the measurement cell is based on the solution of heat balances in the crystallizer, which is considered as an annular heat exchanger. Two types of heat balances are written: an overall balance and a differential balance on each length element dz.

The overall energy balance gives a relationship between the inlet and outlet temperatures of the suspension ($\Delta T_s = (T_3 - T_1)$) and coolant ($\Delta T_e = (T_4 - T_2)$). It is written as follows

$$\Phi_e = -\Phi_s - \Phi_p - \Phi_c \quad (1)$$

so

$$\dot{m}_e c_{p_e} \Delta T_e = -\dot{m}_s c_{p_s} \Delta T_s - \Phi_p - \Delta H_c \frac{dM}{dt}$$

where Φ_e and Φ_s are the heat flows won by the coolant ($\Phi_e > 0$) and lost by the suspension ($\Phi_s < 0$) respectively. Φ_p is the flow of heat loss to the outside (> 0) and Φ_c the heat flow released by crystallization (< 0). Φ_p is estimated using classical correlations representing the heat convection in the annular space, thermal resistance of the glass wall and natural convection at the outside.

The differential balance on one length element dz links together the differences in temperature of the suspension and coolant along the element

$$d\Phi_e = -d\Phi_s - d\Phi_p - d\Phi_c - \dot{m}_e c_{p_e} \frac{dT_e}{dz} =$$

$$-\dot{m}_s c_{p_s} \frac{dT_s}{dz} - \frac{\Phi_p}{L} - \Delta H_c \frac{\partial^2 m}{\partial t\, \partial z} = H_g (T_s - T_e) \frac{dS}{dz} \quad (2)$$

with the following limiting conditions

$$\begin{cases} m(z,t) = 0 \quad z < 0 \text{ and } z > L \\ T_e(0) = T_4 \quad T_s(0) = T_1 \\ T_e(L) = T_2 \quad T_s(L) = T_3 \end{cases}$$

The heat flows exchanged on one length element are written $d\Phi_e$, $d\Phi_s$ $d\Phi_p$ and $d\Phi_c$ respectively for coolant, suspension, loss and crystallization. T_s and T_e are the suspension and coolant temperatures, H_g is the overall heat exchange coefficient and dS is the heat exchange surface of the element. Φ_p is assumed to be constant over the entire crystallizer length, because no crystallization occurs on the external glass tube.

3.2. Modelling of the thermal effects

3.2.1. Before crystallization

As long as no deposit occurs, the heat flow of crystallization does not exist ($\Phi_c = 0$); moreover, the overall heat transfer coefficient H_g and exchange surface S are constant. The differential balance can then be integrated along the length of the tube, leading to the following linear relationship

$$T_3 - T_2 = A(T_4 - T_2) + B \quad (3)$$

In this relationship, coefficients A and B are constant, and the slope A is directly linked with the overall heat transfer coefficient of the system before encrustation H_{g0}. The H_{g0} values obtained are in good agreement with those calculated with classical correlations [7] (Sieder and Tate for the inner tube and Carpenter for the annular space [9]).

3.2.2. Crystallization phase

During this phase, the overall heat exchange coefficient H_g, the heat exchange surface dS and the mean velocity of the suspension vary continuously with the thickness of the deposit. Moreover, the crystallization heat flow must be taken into account; it varies according to the mass flow of crystallization dm/dt. Considering a non uniform thickness along the tube, all the terms of the heat balances become time and space dependent. An analytical integration is therefore impossible, and the numerical solution of the differential balance is performed assuming that the thickness of the layer is constant on each length element. The heat flux of crystallization on one element is then written as follows:

$$d\Phi_c = \Delta H_c \rho (1-\epsilon)\frac{\partial e}{\partial t} dS \quad (4)$$

and

$$dS = 2\pi(r_2 + e)dz$$

The heat exchange surface of the element dS is a function of the external radius of the inner tube r_2, the layer thickness e and the length of the element dz.

A combination of Eqs. (2) and (4) leads to the following differential balance

$$d(T_s - T_e) = [C(T_s - T_e) + D]dS \quad (5)$$

with

$$C = \left(\frac{1}{\dot{m}_e c_{p_e}} - \frac{1}{\dot{m}_s c_{p_s}}\right) H_g(e)$$

$$D = \frac{-\Phi_p}{S(e)\dot{m}_s c_{p_s}} - \frac{\Delta H_c}{\dot{m}_s c p_s}\rho(1-\varepsilon(t))\frac{\partial e}{\partial t}$$

In this relationship, the coefficients C and D are dependent on the constant process parameters (flow rates, specific heats), the layer thickness in the element (through the heat exchange coefficient) and the growth rate of the layer (de/dt). Moreover, the exchange surface of each element dS is dependent on the thickness e of the element. The calculation requires the definition of a thickness evolution law with time and position, which is chosen with regard to the literature and the experimental results (Section 3.4).

Thermal modelling is then based on two calculation loops, one on time (index i) and, for each time step, one on space (index j). At any time, a knowledge of the thickness of one element $e(i,j)$ enables all the terms of the differential heat balance (Eq. (5)), i.e. $H_g(i,j)$, $S(i,j)$, $de/dt(i,j)$, to be calculated, and therefore it is possible to link together the differences in temperature between the suspension and the coolant ($T_s - T_e$) of two successive elements. Step by step, the crystallizer is completely covered, and the overall balance (Eq. (1)) makes the link with the next time step. The calculation steps generally used for time and space are 60 s and 0.01 m respectively. These values were chosen after checking that smaller values do not change the results. Modelling leads to the temperatures and mass crystallized at any time and at any position in the crystallizer. These evolutions can then be compared with our experimental results.

3.3. Thermal effect of fouling

The recording of the inlet and outlet temperatures enables the evolution of the overall heat transfer coefficient between the suspension and the coolant to be followed. Considering the analytical solution of the heat balance without crystallization (Eq. (3)), we chose to plot the difference in temperature between the suspension and the coolant at the top of the crystallizer ($T_3 - T_2$) vs. the variation of the temperature of the coolant along the tube ($T_4 - T_2$). According to Eq. (3), this plot will lead to a straight line before crystallization. An example of some typical curves is given in Fig. 3 for the crystallization of adipic acid on a stainless steel tube at 35°C. The curve is composed of three parts.

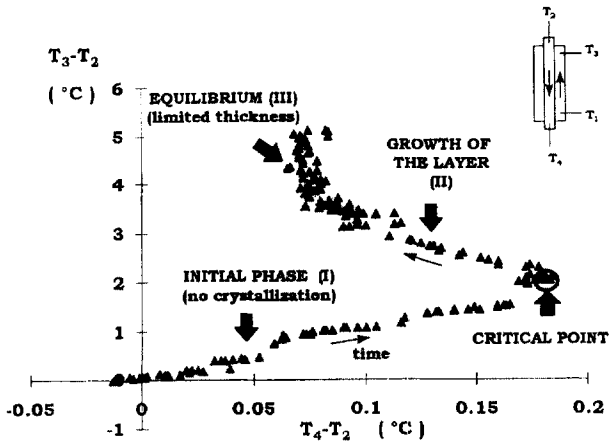

Fig. 3. Evolution of temperature differences.

The initial phase (I), where no crystallization occurs, is represented, as expected, by a straight line. The slope of this line is directly linked with the overall heat exchange coefficient H_{go}.

The second phase (II) shows the evolution of the temperatures during the growth of the layer. The transition between phases (I) and (II) is marked by a return point, representing the thermal effect of fouling. It corresponds to the beginning of the decrease in the overall heat exchange coefficient and allows the critical difference in temperature to be determined.

From this point, the thickness of the layer increases continuously until the system reaches a new equilibrium, represented by the last phase (III). The thickness of the crystalline layer has then reached a limiting value e^* and can be considered as constant, due to the removal of newly formed crystals by high shear stresses.

3.4. Evolution of the layer thickness

Fouling is generally supposed to be the result of the competition between deposition and removal, due to the shear stress caused by the flow of suspension and the erosion of the layer [3–10]. When the rates of these two phenomena are equal, the thickness of the layer reaches a limiting value [2]. We have checked this assumption experimentally. Indeed, all the runs carried out for a sufficient time (above 150 min) show the presence of a final thermal equilibrium representing a limiting thickness, such as phase (III) in Fig. 3. There are two possible main reasons for the achievement of such an equilibrium. During the growth of the layer, the thermal resistance increases, leading to a decrease in supersaturation. The mass flux of crystallization is then considerably reduced. At the same time, the cross-section of the suspension is reduced. Thus, its mean velocity increases, as does the shear stress exerted by the fluid on the layer.

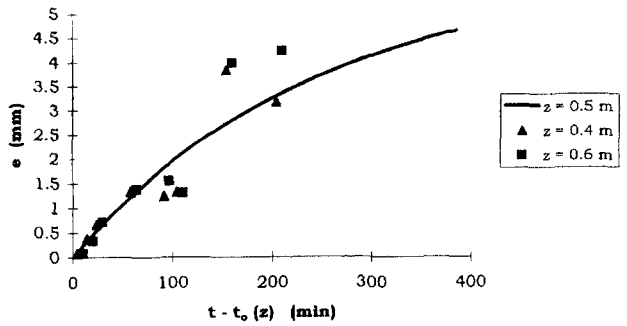

Fig. 4. Calculated and experimental evolution of the layer thickness.

The evolution of the thickness is usually represented by an exponential curve with an asymptotic limit when the rate of removed solids equals that of deposition [2]. Moreover, the experimental results shown that the thickness of the layer is a function of the position on the tube because of the crystallization front.

Taking into account all of these observations, the chosen evolution model is as follows [2]

$$e(z,t) = e^*[1 - \exp(-K(t - t_0(z)))] \quad (6)$$

The expression $t_0 = f(z)$ is that deduced from the observations of the crystallization front during the experiments. The parameters e^* and K are obtained by identification from the evolution of the total mass crystallized vs. time. These parameters are mean values because they are dependent on the suspension velocity, which itself is dependent on the thickness of the layer and, therefore, on the time and position. These mean values are used because they allow the experiment to be represented correctly in terms of the mass of crystallized solid at the end of the experiment and the heat exchanges [7]. An example of the evolution of the thickness with time is given in Fig. 4 for the crystallization of adipic acid on a stainless steel tube at 35°C. The curve plotted in Fig. 4 represents the evolution of the thickness, calculated using Eq. (6), for the position $z = 0.5$ m (middle of the tube). It can be compared with the experimental points, measured at positions $z = 0.4$ and $z = 0.6$ m. From this graph, it can be seen that Eq. (6) correctly represents the experiment, in spite of the simplifications performed.

In this study, parametric identification led to the following laws of evolution for the two chemicals studied:

adipic acid

$$e(z,t) = 5.9 \times 10^{-3}[1 - \exp(-6.7 \times 10^{-5}(t - (6060 - 2400\sqrt{z})))], \quad (7)$$

hydroquinone

$$e(z,t) = 1.3 \times 10^{-3}[1 - \exp(-6.2 \times 10^{-4}(t - (9960 - 3600\sqrt{z})))] \quad (8)$$

These equations are written using SI units.

3.5. Initial kinetics of crystallization

The initial rate of formation of the layer can be deduced from the initial slopes of the curves of the thickness vs. time. Indeed, the initial mass flux of crystallization is calculated by

$$\Phi_{m0} = \rho(1 - \varepsilon_0)\left(\frac{\partial e}{\partial t}\right)_{t=t_0} = \rho(1 - \varepsilon_0)e^*K \quad (9)$$

The term $(\partial e/\partial t)t = t_0$ represents the initial slope of the thickness curves measured experimentally. This slope is measured for each position z on the curve representing the evolution of thickness vs. $(t - t_0(z))$, as shown in Fig. 4. Experimentally, we measured the thickness every 0.05 m, therefore obtaining 20 curves of the evolution of thickness with time, and 20 initial slopes. In the case of adipic acid, all the slopes were similar, and so we considered a single value. In contrast, for hydroquinone, we measured different slope values depending on the position on the tube. These slopes can also be calculated from the chosen law of thickness evolution, by derivating Eqs. (7) or (8) at time t_0. We simply obtain the product (e^*K) (right part of Eq. (9)).

Thermal modelling leads to mean values of the initial layer growth rate. To obtain a more fundamental model, we have attempted to link these values with those obtained using the growth kinetics of the corresponding crystals in suspension, these being inferred from the literature [11–13].

4. Simulation of the initial kinetics of layer growth

To simulate the layer growth rate, we used the growth rates of the crystals obtained from suspension crystallization [11–13]. Our thermal model provides a knowledge of the temperatures at any time and at any position in the crystallizer. It is possible to calculate, from the initial time t_0, the evolution of supersaturation with position. We can then estimate an initial profile of the mass flux of crystallization using the kinetics of crystallization in suspension from the literature. This profile can be compared with that obtained from Eq. (9).

The growth of crystals in suspension is the result of two major steps: the transport of solute by diffusion to the crystal growth surface in the boundary layer, and the integration of the molecules of solute into the crystal lattice [14,15]. The expressions of the molar fluxes for these two steps are as follows

$$\Phi_d = k_d(C - C_i) \quad \Phi_r = k_r(C_i - C^*)^n \quad (10)$$

where C and C_i are the concentrations of solute in the solution and at the interface and C^* is the saturation concentration at the interfacial temperature. The constants k_d and k_r are the coefficient of mass transfer and the kinetic constant of the integration process respectively. The exponent n of the integration kinetics depends on the mechanism of surface integration of the solute in the crystal.

For steady state at the crystal surface, there is no accumulation at the interface, and the two molar fluxes Φ_r and Φ_d are equal (Φ). Using the concept of the effectiveness factor of integration η_r of Garside [16], the equality of the two fluxes leads to the following equation

$$\left[\frac{k_r}{k_d}(C-C^*)^{n-1}\right]\eta_r+\eta_r^{1/n}-1=0 \quad (11)$$

and

$$\eta_r=\frac{\Phi}{k_r(C-C^*)^n}$$

These models are applied to the crystal layers. With our thermal model, we obtain the supersaturation in the form of temperature differences. We can then calculate the term $(C-C^*)$ and enter it into Eq. (11) to estimate the mass flux of crystallization. Examples of such an estimation are shown below for the two chemicals studied, and for the initial growth rate of the layer.

4.1. Adipic acid

The growth kinetics of adipic acid in suspension are given by David et al. [11]

$$\Phi_d=k_d(C-C_i)$$
$$\Phi_r=k_r(C_i-C^*)^2 \quad (12)$$

and

$$k_r=5.26\times10^{14}\exp\left(-\frac{11\,500}{T}\right) \quad (13)$$

where T is the crystallization temperature, fixed for our example at a mean value of 35°C. The kinetic coefficient k_r is then calculated using Eq. (13): $k_r=3.2\times10^{-2}\,\mathrm{mol^{-1}\,m^4\,s^{-1}}$. We can then estimate the coefficient of mass transfer k_d, with the help of an empirical relation established by analogy between heat and mass transfer in an annular space [2]

$$\mathrm{Sh}=0.034\mathrm{Re}^{0.875}\mathrm{Sc}^{0.33}=k_d\frac{D_h}{\mathscr{D}} \quad (14)$$

The physical properties of adipic acid in solution (viscosity, diffusivity) are given by Marchal [12] as a function of the temperature. The application of Eq. (14) in our conditions leads to: $k_d=8.8\times10^{-5}\,\mathrm{m\,s^{-1}}$.

The supersaturation profile at time $t=t_0(z)$ is obtained from the thermal model of the measurement cell [7], using the thickness evolution corresponding to adipic acid (Eq. (7)). The calculation described in Section 3.2. allows the difference in temperature between the suspension and the coolant (T_s-T_e) as a function of the position z to be determined at any time. We can then calculate the difference in temperature between the suspension and the layer surface (T_s-T_p) using the following relationship

$$(T_s-T_p)(z)_{t=t_0}=(T_s-T_e)(z)_{t=t_0}\frac{H_g(z)_{t=t_0}}{H_s(z)_{t=t_0}} \quad (15)$$

where H_s is the heat exchange coefficient of the annular space, and is a function of position z because of the thickness and velocity profile. The time t_0 is the start of layer growth; it is also a function of z because of the crystallization front.

The difference in temperature between the suspension and layer surface represents the supersaturation at the interface, which must be written using a difference of concentrations. The linearization of the solubility equation around the crystallization point leads to a relation between the difference in temperature (T_s-T_p) and the difference in concentration $(C-C^*)$. The solubility of adipic acid is given by Marchal [12]

$$C^*=96.2\times10^7\exp\left(-\frac{4634}{T}\right) \quad (16)$$

where C^* is the molar concentration ($\mathrm{mol\,m^{-3}}$) and T is the temperature (K). The initial evolution of the temperature difference as a function z, obtained by the model is as follows

$$(T_s-T_p)(z)_{t=t_0}=2.1-0.9\sqrt{z}. \quad (17)$$

Finally, we obtain the following initial supersaturation profile

$$(C-C^*)(z)_{t=t_0}=28.2-11.9\sqrt{z} \quad (18)$$

where C and C^* are the molar concentrations ($\mathrm{mol\,m^{-3}}$) and z is the position variable, expressed in metres, with $z=0$ at the bottom and $z=1$ at the top of the crystallizer.

The molar flux of crystallization is then calculated using Eqs. (11) and (18), and converted into the mass flux. However, we can first calculate the effectiveness factor at different positions on the tube, to show that diffusion is the limiting step of growth. Indeed, this effectiveness factor is very low along the entire length of the exchanger: $\eta_r(z=0)=2.6\times10^{-3}$ and $\eta_r(z=1)=2.8\times10^{-3}$. The relation giving the mass flux can then be simplified as follows, in SI units:

$$\Phi_{m0}\approx k_d(C-C^*)=3.62\times10^{-4}-1.53\times10^{-4}\sqrt{z} \quad (19)$$

The evolution of this initial mass flux of crystallization as a function of position is represented in Fig. 5. The experimental value of this flux (see Section 3.5) is also given in

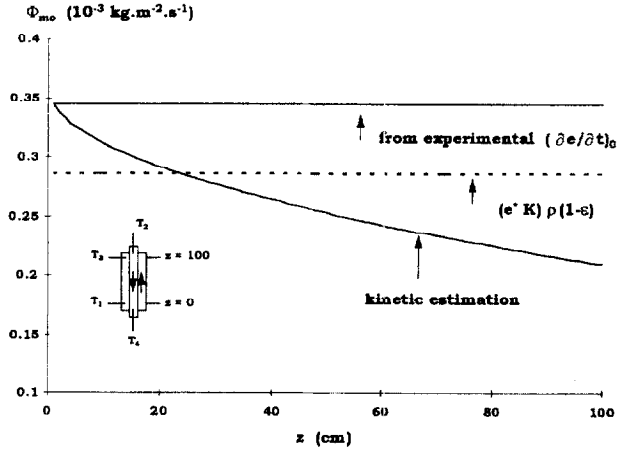

Fig. 5. Initial mass flux of crystallization, adipic acid.

Fig. 5, as well as that obtained from the product (e^*K). The curve denoted as 'kinetic estimation' corresponds to that obtained by introducing the supersaturation profile (Eq. (18)) into the kinetic equation of growth in suspension (Eq. (12)). The experimental value is deduced from the slopes of the thickness curves (see Section 3.5). The broken line is obtained by derivation of the law of thickness evolution, the product (e^*K) representing the slope of the model thickness curves. The corresponding value of the mass flux (broken line) is thus directly dependent on the chosen law of thickness evolution. It represents a mean value in comparison with the kinetic estimation. This is a logical result because the estimation of the flux uses the supersaturation profile obtained with the chosen parameters e^* and K in the thickness model. Therefore the fluxes obtained by kinetic estimation and from the calculated rate of growth of the layer (product e^*K) are closely linked.

With adipic acid, the experimental curves of the thickness at different positions z have the same initial slope. This means that the initial mass flux is independent of the position on the tube, and is represented by the straight line in Fig. 5. This experimental determination of the mass flux lacks accuracy, and there may be an evolution with position that cannot be seen on our curves. However, this experimental value is close to the kinetic estimation at the bottom of the tube (entry of suspension, $z=0$). From this graph, we can conclude that there is quite good agreement between the experimental rate of layer growth and the kinetics of crystalline growth in suspension.

4.2. Hydroquinone

The growth of hydroquinone has been modelled by Puel [13], taking into account the particular shape of the crystals. These are like needle shaped, and can be modelled by a rectangular parallelepiped as represented in Fig. 6. The crystal is characterized by two dimensions, defining two faces (types 1 and 2), which have different kinetics of growth. The growth of face 1 is much faster than that of face 2.

The mass transfer and diffusion coefficient are assumed to be the same for the two types of face [13]

$$\Phi_{d1}=k_d(C-C_{i1}) \quad \Phi_{d2}=k_d(C-C_{i2}) \tag{20}$$

where C_{i1} and C_{i2} are the interfacial concentrations on faces 1 and 2 respectively. The coefficient of diffusion is estimated using the same correlation as for adipic acid (Eq. (14)), employing the physical properties of hydroquinone:

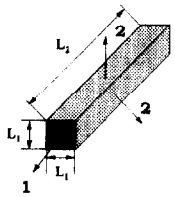

Fig. 6. Model of hydroquinone crystal.

$k_d=1.07\times10^{-4}$ m s^{-1}. The flux of integration of the solute is defined differently for each face [13]

$$\Phi_{r1}=k_{r1}(C_{i1}-C^*)^2 \qquad \Phi_{r2}=k_{r2}(C_{i2}-C^*) \tag{21}$$

The values of the kinetic constants k_{r1} and k_{r2} are given by Puel [13] at 25°C (Eq. (21)): $k_{r1}=2.75\times10^{-6}$ mol m^4 s^{-1}; $k_{r2}=1.05\times10^{-5}$ m s^{-1}.

For faces of type 1, the overall flux of crystallization is given by a relation similar to Eq. (11). The difference in this case is that neither diffusion nor integration is limiting, so that the equation cannot be simplified, and leads to the following expression of the initial mass flux in SI units

$$\Phi_{m02}=2.3\times10^{-4}+1.18\times10^{-5}(C-C^*) - 1.18\times10^{-5}\sqrt{378+38.9(C-C^*)} \tag{22}$$

For faces of type 2, the equality of the diffusion and integration flux allows the following relationship to be obtained

$$\Phi_{m02}=1.06\times10^{-6}(C-C^*) \tag{23}$$

The evolution of the thickness of the layer differs from that in the case of adipic acid (Eq. (8) for hydroquinone), but the principle of calculation leading to the supersaturation profile is exactly the same. The solubility of hydroquinone in the range of temperature used is given by Puel [13]

$$C^*=1.76\times10^5\exp\left(-\frac{3044}{T}\right) \tag{24}$$

The supersaturation profile is then given by the following equation in SI units

$$C-C^*=93.1-44\sqrt{z} \tag{25}$$

The initial crystallization flux is represented for the two types of face in Fig. 7. In this case, the experimental value of the flux depends on the position z. We have distinguished four zones, corresponding to four different initial slopes of the curves of thickness vs. time: p_1, p_2, p_3, p_4 for $z<0.2$, $0.2<z<0.4$, $0.4<z<0.8$ and $z>0.8$ m respectively.

The graph in Fig. 7 shows that the experimental rates of formation of the layer correspond to intermediate values between the kinetics of growth of the two types of face. The asymmetrical shape of the crystal is of great importance. Indeed, the evolution of the thickness of the layer corresponds to growth in the radial direction. According to the orientation of the crystals on the exchange surface, the radial growth will be that of face type 1 or 2. If the needles are tangential (lengthwise) to the heat exchange surface, the radial growth will be that of face 2. In contrast, if the needles are perpendicular to the surface, the growth of the layer will correspond to that of face 1 which is much faster.

To obtain more information about the orientation of the crystals, we took some photographs of the initial deposit, see (Fig. 8). To obtain these pictures, we stopped the experiment just after the first crystals had been deposited, and carefully removed the inner tube to observe its surface under the micro-

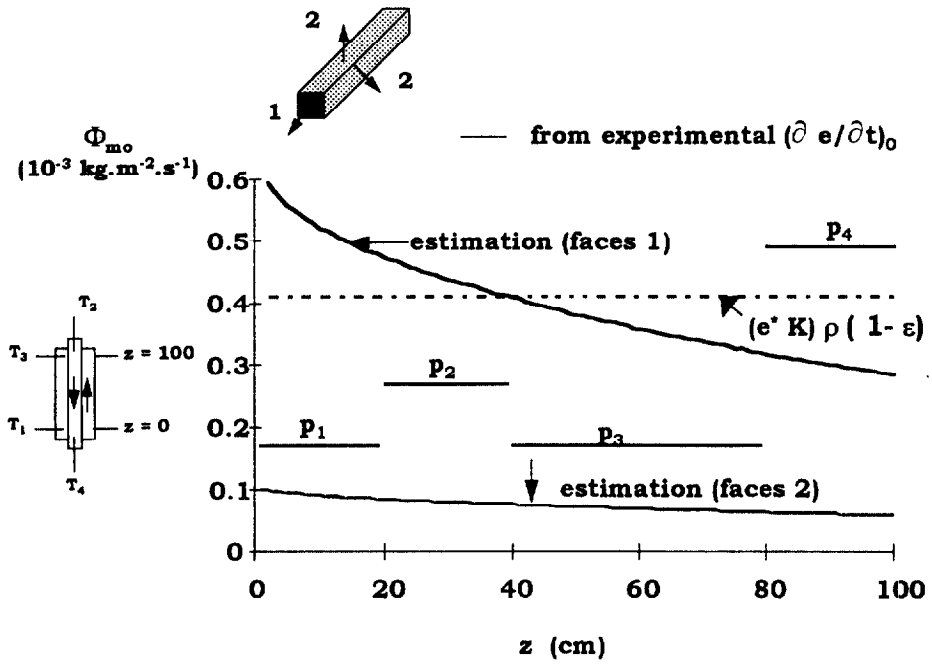

Fig. 7. Initial mass flux of crystallization, hydroquinone.

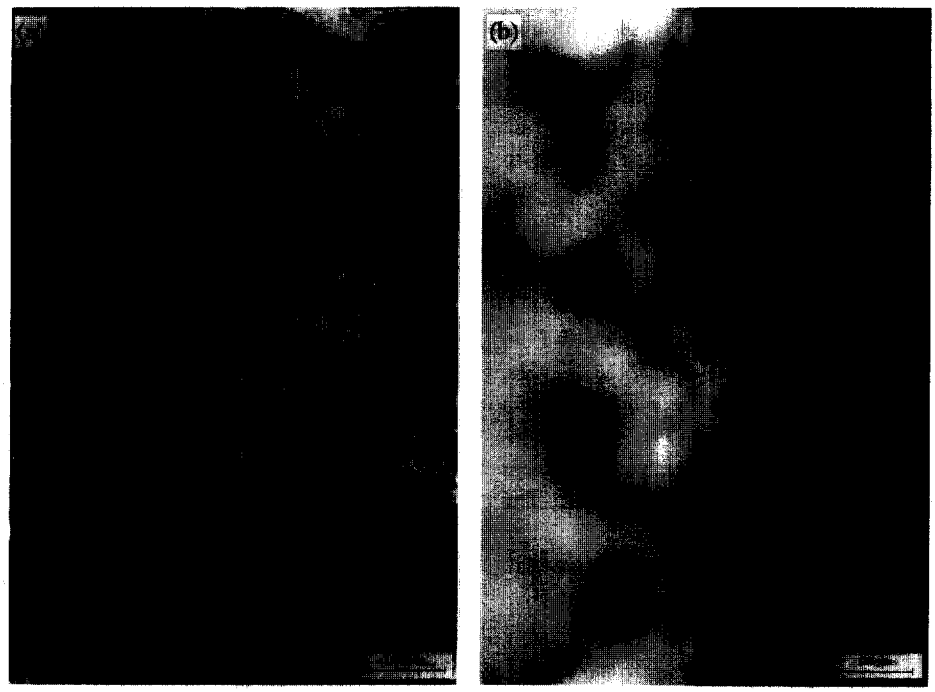

Fig. 8. Photographs of the initial deposit, hydroquinone: (a) front view; (b) side view.

scope. It can be seen that the majority of crystals lie in the plane of the heat exchange surface, but there are some needles perpendicularly disposed. These observations show that we measured a rate of formation of the layer corresponding to the kinetics of crystalline growth of the two types of face.

The flux obtained from the product e^*K (broken line) is a mean value corresponding to the estimation of the growth of face 1. However, our experimental observations show that the growth of the layer corresponds to an intermediate value between the growth of faces 1 and 2. It should be noted that parameters e^* and K vary position z and time. The mean values used allow the experiments to be represented, but only lead to an approximation of the initial flux.

5. Conclusions

The experimental study enabled the influence of the most important parameters on the initiation of fouling to be determined, together with its further development and its effects

on heat exchange. Empirical relations of the evolution of the main measurements were proposed, and were used for thermal modelling. These model was based on the choice of an empirical law of the evolution of the layer thickness with time and position, according to the experimental results and the literature. The identification of parameters as a function of the experimental evolution of the crystallized solid with time validates the choice of an exponential model with an asymptotic limit.

Initially, we simplified the model by assuming that the parameters e^* and K of the thickness law were constant, and used mean values to represent the experiment. More fundamental modelling requires the use of crystallization kinetics and, consequently, a knowledge of the supersaturation as a function of time and space. As a first attempt, we used our empirical model to calculate the initial supersaturation, and applied growth kinetics from the literature with this supersaturation to estimate the initial growth rate of the layer. The simulations were then compared with the experimental kinetics. Concerning the beginning of crystallization, good agreement was obtained between the experimental rate of formation and that deduced from the kinetics of crystalline growth in suspension.

This process allowed the model to be validated in spite of the simplifying assumptions made. In the case of hydroquinone, the rate of growth of the layer is close to that of the faces of larger length. This means that the crystals are tangential to the exchange surface. This was confirmed by photographs taken at the start of formation of the layer, which show that the majority of crystals are tangential (lengthwise) but that some are perpendicularly oriented. This explains the intermediate rate of formation found experimentally. These observations demonstrate the importance of the initial phase of fouling, especially with regard to the orientation of the crystals on the heat exchange surface. The thermal model could be modified to represent this initial phase more accurately. The production of general model is in progress.

Appendix A. Nomenclature

C	solution concentration	(mol m^{-3})
C^*	saturation concentration at the interfacial temperature	(mol m^{-3})
C_i	interfacial concentration	(mol m^{-3})
c_p	specific heat	(J kg^{-1} K^{-1})
D	molecular diffusivity of solute	(m^2 s^{-1})
D_h	hydraulic diameter	(m)
dS	exchange surface of one length element	(m^2)
dT	temperature difference of one element	(K)
dz	length of one element	(m)
e	thickness of the layer	(m)
e^*	parameter of the law of thickness evolution	(m)
H_g	overall heat exchange coefficient	(W m^{-2} K^{-1})
K	parameter of the law of thickness evolution	(s^{-1})
k_d	coefficient of mass transfer	(m s^{-1})
k_r	kinetic constant of integration process	(mol^{1-n} m^{3n-2} s^{-1})
L	length of the crystallizer	(m)
$\dot{m}$	mass flow rate	(kg s^{-1})
m	mass deposited on one length element	(kg)
M	mass deposited on the whole tube	(kg)
r_2	external radius of the inner tube	(m)
Re	Reynolds number	
Sc	Schmidt number	
Sh	Sherwood number	
T	temperature	(K)
t	time	(s)
t_0	induction time	(s)
z	position on the tube	(m)

Greek symbols

ε	porosity of the layer	
ΔH_c	heat of crystallization	(J kg^{-1})
$d\Phi$	heat flow on one length element	(W)
Φ	heat flow	(W)
Φ_d	diffusion molar flux	(mol m^{-2} s^{-1})
Φ_{mo}	initial mass flux	kg (m^{-2} s^{-1})
Φ_r	integration molar flux	(mol m^{-2} s^{-1}
ρ	density of the solid	(kg m^{-3})
η_r	effectiveness factor of integration step	

Index

e	coolant (water)
s	suspension
c	crystallization
p	loss to the outside

References

[1] E.F.C. Somerscales, Heat Transfer Eng. 11 (1) (1990) 19–36.
[2] S. Krause, Int. Chem. Eng. 33 (3) (1993) 355–401.
[3] J. Taborek, T. Aoki, R.B. Ritter, J.W. Palen, J.G. Knudsen, Chem. Eng. Prog. 68 (2) (1972) 59–67.
[4] J. Taborek, T. Aoki, R.B. Ritter, J.W. Palen, J.G. Knudsen, Chem. Eng. Prog. 687 (1972) 69–78.
[5] D.H. Troup, J.A. Richardson, Chem. Eng. Commun. 2 (1978) 167–180.
[6] R.A.W. Shock, J. Separation Processes Technol. 4 (1983) (1), 1–13.
[7] S. Briançon, Etude expérimentale et modélisation du blindage en cristallisation industrielle, PhD Thesis, Université Claude Bernard Lyon 1, Lyon, France, 1996.
[8] S. Briançon, D. Colson, J.P. Klein, Chem. Eng. Res. Design (Trans. Inst. Chem. Engineers Part A) 75 (1997) 147–151.

[9] J.P. Taine, J.P. Petit, Transferts Thermiques, Dunod, Paris, 1989.
[10] N. Epstein, Heat Transfer Eng. 4 (1) (1983) 43–56.
[11] R. David, J. Villermaux, P. Marchal, J.P. Klein, Chem. Eng. Sci. 46 (4) (1991) 1129–1136.
[12] P. Marchal, Génie de la cristallisation: Application à l'acide adipique, PhD Thesis, Institut National Polytechnique de Lorraine, Nancy, France, 1989.
[13] F. Puel, Bilan de population pour deux tailles caractéristiques des particules: application à la cristallisation de l'hydroquinone, PhD Thesis, Université Claude Bernard Lyon 1, Lyon, France, 1994.
[14] S.J. Jancic, P.A.M. Grootscholten, in: D. Reidel (Ed.), Industrial Crystallization, Delft Univ. Press, 1984.
[15] A. Mersmann, in: A. Mersmann (Ed.), Crystallization Technology Handbook, Marcel Dekker, 1995.
[16] J. Garside, Chem. Eng. Sci. 26 (1971) 1425–1431.